# Melbourne multi-sensor urban positioning and mapping dataset

Junjie Zhang[1,2], Marko Radanovic[2], Yuan Zhao[2], Amir Khodabandeh[2], Kourosh Khoshelham[2]

[1] School of Science, Engineering and Digital Technologies, University of Southern Queensland, Springfield, Queensland, Australia - Desmond.Zhang@unisq.edu.au
[2] Department of Infrastructure Engineering, The University of Melbourne, Parkville, Victoria, Australia - (junjzhang@, m.radanovic@, k.khoshelham@, yuan.zhao1@student., akhodabandeh@)unimelb.edu.au

**Keywords:** Global Navigation Satellite System, Inertial Navigation System, Lidar, Mapping, Multi-Sensor Dataset, Positioning and Navigation.

**Abstract**

Reliable positioning and mapping in dense urban environments remain challenging due to signal blockage, multipath, and dynamic scenes. Progress on multi-sensor integrated positioning and visual/lidar SLAM has been driven by open datasets, yet most existing resources are either perception-centric with limited raw navigation data, focused on controlled environments, or built around outdated software platforms and/or data formats. In this paper, we present the Melbourne Multi-Sensor Urban Positioning and Mapping Dataset, a new resource targeting urban vehicle navigation and mapping tasks. The dataset was collected using a custom mobile mapping platform equipped with a tactical-grade INS, a survey-grade Leica GNSS receiver, a low-cost UBLOX GNSS receiver, a high-resolution Ouster OS1 128 lidar, and four industrial FLIR cameras providing 360° coverage. Seven data collection trips were recorded on dynamic streets in several inner suburbs of Melbourne, including multiple closed loops and a repeated route with day–night variation. For better compatibility and future-proofing, all raw data are provided as standard ROS2 message streams in MCAP format, complemented by commonly used individual formats and GNSS products for multi-sensor integrations. We benchmark three GNSS–based positioning packages (RTKLib, Net_Diff and Ginan) and four state-of-the-art lidar(-inertial) odometry/SLAM methods (FAST-LIO2, KISS-ICP, KISS-SLAM and PIN-SLAM), demonstrating the applicability and compatibility of our dataset for modern positioning and mapping software pipelines. The dataset is designed as a robust, ROS2-native testbed for research on GNSS/IMU/lidar/camera fusion for the testing and validation of vehicle positioning and mapping in urban environments, which is available open-source at `https://github.com/zjjdes/melbourne_dataset`.

## 1. Introduction

Worldwide efforts on the innovation of autonomous driving in recent years are pushing it to become a reality (Zhao et al., 2024). Among the core components of autonomous driving systems, positioning and mapping remain fundamental elements to facilitate vehicle navigation, control and safety. It has been well established that accurate and reliable vehicle positioning requires the integration of multiple sensors, including but not limited to Global Navigation Satellite System (GNSS), Inertial Measurement Unit (IMU), various types of cameras and Lidar to combat environmental dynamics and constraints (Zhang et al., 2023b, Schaper and Schön, 2024, Hsu et al., 2025). Several branches of multi-sensor vehicle positioning and mapping methods have been studied and developed, such as GNSS–inertial integration (Budiyono, 2012), GNSS–camera/lidar integration (Cao et al., 2022, Zhang et al., 2023a), visual/lidar(–inertial) odometry (Ramezani and Khoshelham, 2018, Shan and Englot, 2018, Xu et al., 2022), visual/lidar Simultaneous Localisation and Mapping (SLAM) (Wang et al., 2024, Pan et al., 2024), etc., while new advances are constantly being made to their accuracy, reliability and continuity.

The validation and benchmarking of these methods are crucial for evaluating and comparing their performance in challenging urban environments, for which open-source datasets have played a key role historically. The KITTI dataset published in 2013 is one of the earliest of such works, which consists mainly of imagery and lidar point cloud data and has been widely used to study, e.g., environmental perception and visual/lidar odometry (Geiger et al., 2013). More datasets have since been created to incorporate more types of sensors and more modern hardware and software standards. For instance, nuScenes and Waymo datasets focus on computer vision tasks with images and point clouds (Caesar et al., 2020, Sun et al., 2020), but do not provide the raw sensor data needed for positioning. M2DGR and The University of Michigan North Campus Long-Term Vision and LIDAR (NCLT) dataset are widely used for lidar mapping as they are collected in controlled environments rather than urban roads (Yin et al., 2022, Carlevaris-Bianco et al., 2016). The Perth dataset is one of the first collected in Australia in the southern hemisphere, focusing on lidar mapping of the central city of Perth (Ibrahim et al., 2021). Novel sensor types are being explored as well such as event cameras found in the ECMD dataset (Chen et al., 2023). Finally, UrbanNav and NavINST represent the breed of datasets with an emphasis on positioning, by providing high-frequency raw observations from IMU and GNSS devices to allow deep integration of multiple sensors (Hsu et al., 2023, Araujo et al., 2025). In addition, some of these datasets adopt Robot Operating System (ROS) to enable data synchronization and standardisation. However, their data formats are associated with ROS version 1, which has been deprecated in favour of version 2 (Macenski et al., 2022), which supports more modern message types and software pipelines.

In this paper, we present the Melbourne Multi-Sensor Urban Positioning and Mapping Dataset. We aim to provide a complete, standardised, robust and future-proof platform for positioning and mapping research, which will require minimal effort to be deployed on the software implementations of modern multi-sensor integrations. The main contributions of this data-

This contribution has been peer-reviewed. The double-blind peer-review was conducted on the basis of the full paper.
https://doi.org/10.5194/isprs-annals-XI-1-2026-35-2026  

set include:

- Multi-sensor data were collected using redundant GNSS, IMU, cameras and lidar devices on the urban streets of Melbourne, Australia.
- We utilise 360° of camera view, very high lidar point cloud density, very high IMU frequency and triple-frequency GNSS observations to maximise the flexibility of using this dataset for various objectives.
- Raw data have been retained from all sensors to enable tight coupling, including multi-system multi-frequency GNSS observations.
- Data collection included closed loops and repeated trajectories to facilitate global optimisation.
- In addition to conventional file formats, all data are provided in the latest MCAP format to be compatible with modern ROS2 workflows.

The remainder of this paper proceeds as follows: Section 2 reviews representative existing datasets used for positioning and mapping. Section 3 describes the hardware platform used for data collection. The structure and formats of the dataset are outlined in Section 4, while positioning benchmarks using state-of-the-art methods on our dataset are provided in Section 5. Finally, Section 6 and Section 7 discuss the limitations of the dataset and concluding remarks.

## 2. Related work

The development of positioning and mapping methods for autonomous driving has been historically enabled by open-source multi-sensor datasets. Early efforts such as the KITTI dataset combine stereo cameras and a Velodyne lidar with GNSS/IMU information and have been widely used for benchmarking visual/lidar odometry and perception tasks including object detection and tracking (Geiger et al., 2013). Oxford RobotCar extended this paradigm to repeated traversals of the same routes over more than a year, enabling long-term localisation studies under changing weather and lighting (Maddern et al., 2017). Most autonomous driving datasets place a stronger emphasis on 3D perception with high-definition lidar and rich camera configurations. nuScenes and the Waymo Open Dataset, for example, provide large-scale, accurately annotated point clouds and images for 3D detection, tracking and prediction tasks (Caesar et al., 2020, Sun et al., 2020). While these datasets have been extremely influential, their navigation components are typically limited to processed poses or reference trajectories without raw multi-frequency GNSS or high-rate IMU observations needed to study tightly coupled or deeply integrated navigation algorithms, and they pre-date modern software frameworks such as ROS2. Other datasets have focused specifically on SLAM in ground-robot scenarios. The M2DGR dataset targets multi-sensor and multi-scenario SLAM for ground robots with cameras, IMU and lidar in a variety of indoor and outdoor scenes (Yin et al., 2022). The University of Michigan NCLT dataset further emphasises long-term operation using lidar, camera and IMU measurements, while it is constrained in a campus environment rather than dense urban street canyons (Carlevaris-Bianco et al., 2016).

Several works explicitly address challenging urban navigation and high-precision positioning. The Perth CBD dataset provides high-definition lidar mapping of an Australian central business district, focusing on large-scale 3D mapping using a high-end lidar on a vehicle platform (Ibrahim et al., 2021). Hong Kong UrbanNav offers a multi-sensor dataset collected in various depths of urban canyons, integrating different grades of GNSS receivers, IMU, lidar and cameras with an emphasis on benchmarking urban GNSS and multi-sensor navigation algorithms (Hsu et al., 2023). More recently, the NavINST dataset has been introduced as a multi-sensor autonomous navigation dataset with multiple lidars, radars, cameras and high-end GNSS/IMU, fully integrated in ROS, to support research on high-precision positioning and multi-sensor fusion (Araujo et al., 2025). The ECMD dataset explores the use of event cameras alongside standard cameras, lidar and GNSS/IMU in challenging driving scenarios, pushing the envelope of sensor modalities used for urban navigation (Chen et al., 2023).

As summarised in Table 1, these datasets differ in their sensor configurations, environments, and software implementations. Some provide raw GNSS and IMU data but focus on campus or controlled settings, while others target dense urban scenes but are perception-centric and lack full access to raw navigation measurements. Moreover, most existing datasets rely on ROS1 and its associated data formats that are now retired (Macenski et al., 2022). In contrast, the Melbourne Multi-Sensor Urban Positioning and Mapping Dataset is designed to combine redundant GNSS receivers, a tactical-grade INS, a high-resolution 3D lidar and 360° camera coverage in GNSS-challenged urban environments, while natively recording all streams as standard ROS2 messages in the MCAP format. By retaining raw GNSS observations, high-rate inertial data and dense lidar and camera outputs, our dataset complements existing resources and provides a modern, future-proof platform for research on tightly integrated positioning, GNSS augmentations, and urban SLAM.

## 3. Multi-sensor mobile mapping platform

### 3.1 Hardware configuration

The mobile mapping platform used in this work is custom-made with aluminium extrusions to provide stable housing for the sensors, which are positioned to optimise visibility. Table 2 provides the details of the sensors and their data output. A tactical-grade Inertial Navigation System (INS), VectorNav VN300, is used to record IMU observations at 400 Hz and ground truth WGS84 coordinates, thanks to its centimetre-level accuracy leveraging GNSS–inertial positioning with two GNSS antennas. Two other GNSS receivers, namely a survey-grade Leica GS18 and a commercial unit UBLOX F9P with an ANN–MB patch on antenna, are used to collect raw GNSS observations from GPS, GLONASS, Galileo, Beidou and QZSS, at triple frequencies (L1, L2, L5) and dual frequencies (L1, L2), respectively. A 3D lidar scanner Ouster OS1 128 with a built-in IMU is installed in the centre of the platform and elevated to avoid obstruction from the vehicle underneath. The point clouds are collected with the resolution of $2048 \times 128$ at 10 Hz, higher than that found in any existing dataset. Four industrial cameras are installed on each side of the platform to complete a 360° view. The front and back cameras are FLIR RGB cameras of 3.2 megapixels (MP), with the former being extended towards the front of the vehicle. The two side cameras are FLIR mono colour of 5 MP. The side and back cameras are slightly pivoted downward to capture more road environments than sky. All cameras output images at the highest available resolutions

Table 1. Positioning and mapping dataset feature comparison.

| Dataset | Raw data | | | | Urban roads | ROS version |
|---|---|---|---|---|---|---|
| | IMU | GNSS | Lidar | Camera | | |
| Oxford RobotCar (Maddern et al., 2017) | | | ✓ | ✓ | ✓ | |
| M2DGR (Yin et al., 2022) | ✓ | ✓ | ✓ | ✓ | | 1 |
| Perth (Ibrahim et al., 2021) | | | ✓ | | ✓ | |
| NCLT (Carlevaris-Bianco et al., 2016) | | | ✓ | ✓ | | 1 |
| nuScenes (Caesar et al., 2020) | | | ✓ | ✓ | ✓ | |
| Waymo (Sun et al., 2020) | | | ✓ | ✓ | ✓ | |
| KITTI (Geiger et al., 2013) | | | ✓ | ✓ | ✓ | |
| UrbanNav (Hsu et al., 2023) | ✓ | ✓ | ✓ | ✓ | ✓ | 1 |
| NavINST (Araujo et al., 2025) | ✓ | ✓ | ✓ | ✓ | ✓ | 1 |
| **Ours** | ✓ | ✓ | ✓ | ✓ | ✓ | **2** |

and the same frequency as lidar. Figure 1 presents the complete mobile mapping platform installed on a Toyota Hilux utility vehicle with a roof rack.

All sensors are connected to a single central computer via high-speed Thunderbolt, USB and/or Ethernet connections. ROS2 is used for recording raw data in standard sensor message types, timestamping and producing a single MCAP file per data collection trip.

### 3.2 Synchronisation and calibration

The four cameras on the mobile mapping platform are synchronised using physical GPIO connections, ensuring that images collected using different cameras simultaneously have identical timestamps. All the sensor messages are given POSIX timestamps and synchronised to the central computer's system time thanks to ROS2, while the INS also records the Global Positioning System (GPS) timestamps in case a time offset exists.

The intrinsic calibration of the four cameras and the IMU within VectorNav VN300 is performed prior to data collection activities. The distortion parameters of each camera are obtained using the calibration tool built into ROS with a checker board target [1], while the Allan variances of the aforementioned IMU are analysed using an open-source tool [2] by recording 4 hours of stationary gyroscope and accelerometer observations.

In order to integrate data obtained from different sensors, the extrinsic transformations between every two of them must be accurately known, which are estimated using state-of-the-art open-source tools in this work. *LI-Init* is utilised for estimating the transformation between the lidar and the INS, which is a real-time lidar–inertial initialisation method that can calibrate temporal offsets and extrinsic parameters by building a point cloud map (Zhu et al., 2022), therefore can be used with collected data without using dedicated targets. The transformations between lidar and the four cameras are estimated using the targetless *direct_visual_lidar_calibration* method (Koide et al., 2023), which performs the calibration using manually identified correspondences between the 3D point clouds and 2D images. The translations from the INS to the two GNSS devices are provided based on the mechanical drawings of the platform. Figure 2 demonstrates the relationships among the extrinsic transformations and their identifiers in the ROS configuration, while Figure 3 presents a simplified visualisation of these transformations as seen from a bird-eye view above the vehicle.

[1] `https://wiki.ros.org/camera_calibration`
[2] `https://github.com/rpng/kalibr_allan`

## 4. Data description

### 4.1 Data collection trips

Using the mobile mapping platform as described in Section 3, 7 data collection trips were conducted in suburbs close to central Melbourne, Australia, including North Melbourne, Richmond, Fitzroy, Clifton Hill and Northcote, where GNSS satellite visibility was challenged by dense buildings near the roads. Each trip lasted between 10 and 20 minutes with the vehicle travelling at an average speed of 40 km/h. Figure 4 visualises the trajectories traversed by these trips generated using the INS output, of which 4 have closed loops, i.e., the vehicle returned to the starting locations, to support loop closures in globally optimised positioning and mapping methods such as visual or lidar SLAM. The first route, namely *20241020*, was recorded twice with the second trip performed in the evening, thus allowing repeatable validations and providing varied lighting conditions for environmental perception studies.

### 4.2 Data formats

In this work, we record all raw data in standard ROS message types, which are then saved in the latest MCAP format so that modern software pipelines developed using ROS2 can seamlessly use this dataset without any data preprocessing. Table 3 lists the message types and topic names of all the usable data included in the MCAP data bags. Note that the raw GNSS observations collected by Leica GS18 are not included in the MCAP files but are kept as separate RINEX 3 files due to its lack of a ROS2 driver.

For better compatibility in software that does not utilise ROS2, we provide all the above data in common individual formats as well. For instance, point clouds are saved in PCD files with intensity values, images are offered as uncompressed BMP files, raw GNSS observations are exported as RINEX 3 files, while all the INS data are provided as CSV files. Every data entry uses the POSIX timestamps as their filenames for convenient synchronisation. Figure 5 demonstrates the visual data output from lidar and the four cameras, highlighting the full field of view of these two types of sensors.

In addition, we include in the dataset GNSS RINEX 3 observations and navigation messages from nearby Continuously Operating Reference Stations (CORS) and State-Space Representation (SSR) products obtained from International GNSS Service (IGS) and Center for Orbit Determination in Europe (CODE), thus enabling the implementations of GNSS-based positioning such as Real-time Kinematic (RTK), Precise Point Positioning (PPP) and PPP–RTK.

Table 2. Sensor specifications of the custom mobile mapping platform.

| Sensor type | Model | Quantity | Frequency [Hz] | Output |
|---|---|---|---|---|
| INS | VectorNav VN300 | 1 | 400 | Inertial measurements, WGS84 coordinates |
| GNSS | Leica GS18 | 1 | 1 | Raw GNSS measurements (GREJC; triple-frequency) |
| GNSS | UBLOX F9P (with ANN–MB antenna) | 1 | 1 | Raw GNSS measurements (GREJC; dual-frequency) |
| Lidar | Ouster OS1 128 | 1 | 10 | 3D point clouds (2048 ×128) |
| Camera | FLIR Blackfly S BFS-U3 3.2 MP colour | 2 | 10 | RGB images (2048 ×1536) |
| Camera | FLIR Blackfly S BFS-U3 5 MP mono | 2 | 10 | Mono images (2448 ×2048) |

Figure 1. Multi-sensor mobile mapping platform.

## 5. Positioning and mapping benchmark results

In order to demonstrate the applicability and compatibility of the dataset, we implemented 7 state-of-the-art positioning methods, loosely categorised as GNSS–based and lidar–based, using data from the *20241021_1* trip collected in Richmond as shown in Figure 4. All implementations were based on their open-source software using default or recommended configurations at the time of writing, as algorithmic optimisation and improvement are not within the scope of this contribution. To evaluate the positioning performance, we computed horizontal, vertical and rotational errors in the East-North-Up (ENU) directions against the ground truth coordinates yielded by the tactical-grade INS using Equation 1, where $\Delta E$, $\Delta N$, $\Delta U$ are the ENU errors, respectively. $\boldsymbol{R}_{est}$ and $\boldsymbol{R}_{gt}$ denote the estimated and ground truth rotational matrices representing the attitudes of the vehicle, while $trace(\cdot)$ is the trace operator of a matrix. These individual positioning errors are then summarised as Root Mean Squared Errors (RMSE) to represent the overall positioning performance.

$$\begin{cases} Horizontal\,error = \sqrt{\Delta E^2 + \Delta N^2} \\ Vertical\,error = \sqrt{\Delta U^2} \\ Rotational\,error = cos^{-1}\left(\frac{trace(\boldsymbol{R}_{est}^T \boldsymbol{R}_{gt}) - 1}{2}\right) \end{cases} \tag{1}$$

We first present the positioning results based on GNSS only using 3 widely adopted GNSS positioning software packages, namely RTKLib (Takasu and Yasuda, 2009) – the most renowned GNSS processing software, Net_Diff (Zhang et al., 2020, Zhang et al., 2019) – a GNSS positioning and analysis package supporting multiple algorithms, and Ginan (McClusky et al., 2024) – feature-rich GNSS Analysis Centre software developed by Geoscience Australia. Where feasible, raw observations from both the survey-grade Leica GS18 and the commercial UBLOX F9P are used for RTK and PPP processing using observations from nearby CORS and final precise satellite orbit and clock corrections produced by IGS. Figure 6 plots the number of observed satellites throughout data collection, which shows that the low-cost UBLOX F9P was able to track more satellites than Leica GS18, partially due to GLONASS being completely unavailable to the latter in this particular collection. However, as a result of the multipath effect and the low signal quality, most of the UBLOX observations were rejected by the outlier filters in the tested software and failed the positioning tasks. Therefore, we only provide the results using UBLOX F9P in the RTK processing in RTKLib, while Leica GS18 data was successfully processed in all three software packages.

Table 4 presents the positioning performance of all tested positioning methods in terms of RMSE, in which the first 5 are GNSS–based. Note that these results do not include rotational errors as standalone GNSS cannot estimate vehicle attitudes. It can be seen that Leica GS18 can achieve metre-level positioning accuracy in both RTK and PPP modes, which is typical for urban kinematic positioning (Zhang et al., 2023b). In contrast, UBLOX F9P performs poorly in dual-frequency RTK in RTK-


Figure 2. Illustration of extrinsic transformations and hardware-level time synchronisations between sensors.

Table 3. ROS message types and topic names of provided raw data.

| Sensor | Data type | Message type | ROS topic |
|---|---|---|---|
| Camera | Camera parameters | sensor_msgs/msg/CameraInfo | /cam_sync/cam0/camera_info |
| | Image | sensor_msgs/msg/Image | /cam_sync/cam0/image_raw |
| Lidar | Inertial | sensor_msgs/msg/Imu | /ouster/imu |
| | Point cloud | sensor_msgs/msg/PointCloud2 | /ouster/points |
| UBLOX GNSS | Position | sensor_msgs/msg/NavSatFix | /fix |
| | Velocity | geometry_msgs/msg/TwistWithCovarianceStamped | /fix_velocity |
| | Raw GNSS | ublox_msgs/msg/RxmRAWX | /rxmraw |
| INS | Position | sensor_msgs/msg/NavSatFix | /vectornav/gnss |
| | Pose | geometry_msgs/msg/PoseWithCovarianceStamped | /vectornav/pose |
| | Inertial | sensor_msgs/msg/Imu | /vectornav/imu |
| | Inertial (uncompensated) | sensor_msgs/msg/Imu | /vectornav/imu_uncompensated |
| | Velocity | geometry_msgs/msg/TwistWithCovarianceStamped | /vectornav/velocity_body |
| | Magnetic | sensor_msgs/msg/MagneticField | /vectornav/magnetic |
| | Temperature | sensor_msgs/msg/Temperature | /vectornav/temperature |

Lib, yielding decimetre-level positioning accuracy due to its lower-performing patch antenna being more severely affected by the challenging environment. Figure 7 shows the time series of the absolute positioning errors, which further demonstrates the environmental influences in the form of sudden increases. The same behaviour can be observed in Figure 8 and Figure 9 as well, which present the 2D and 3D trajectories estimated by the tested positioning methods.

The 4 lidar–based positioning and mapping methods listed below are evaluated. These methods are state-of-the-art contributions in this field which use ROS2 as the implementation platform and have shown competitive accuracy and reliability.

- FAST-LIO2 (Xu et al., 2022): lidar–inertial odometry
- KISS-ICP (Vizzo et al., 2023): lidar odometry
- KISS-SLAM (Guadagnino et al., 2025): lidar SLAM
- PIN-SLAM (Pan et al., 2024): lidar SLAM

It is evident from Figures 8 and 9 that lidar–based methods can generate smoother trajectories comparing with those based on GNSS, due to the core step of them being consecutive point cloud registrations. However, this inevitably leads to estimated poses drifting over time. Figure 7 demonstrates that lidar–based methods tend to have significantly larger translational errors after the vehicle has been travelling for only a few minutes. It also causes the RMSE values in Table 4 to imply that lidar–based positioning methods are much more inaccurate than GNSS–based ones, while Figure 7 shows it is the increased errors over time hiding the fact that their accuracy is high at the beginning or upon loop closures.

Despite being one of the best-performing lidar odometry methods, KISS-ICP shows the worst overall positioning performance among all the tested methods because of the lack of inertial measurements or global optimisation such as loop closures. With the additional input of an IMU, FAST-LIO2 sees a 26% improvement in horizontal RMSE. However, Figure 8 shows that both methods suffer heavily from drifting over time and would be unsuitable for large-scale mapping tasks. In comparison, KISS-SLAM and PIN-SLAM further improve accuracy by leveraging factor graph optimisation with loop closures, correctly leading the trajectories back to the starting locations.

This contribution has been peer-reviewed. The double-blind peer-review was conducted on the basis of the full paper.
https://doi.org/10.5194/isprs-annals-XI-1-2026-35-2026 | © Author(s) 2026. CC BY 4.0 License.

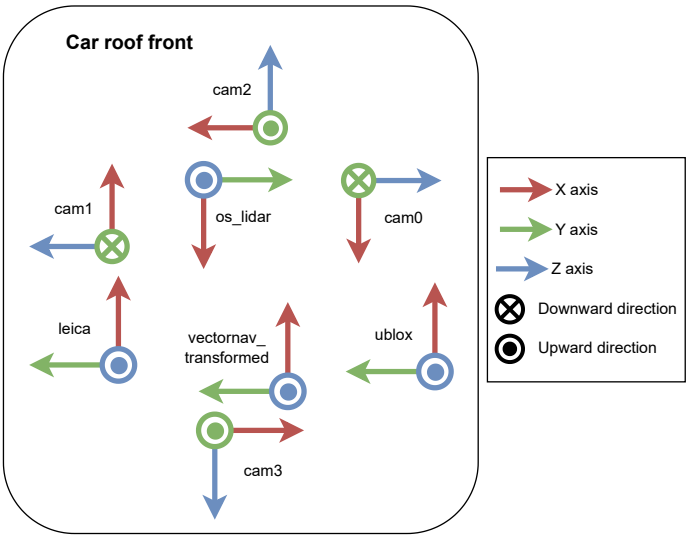


Figure 3. Top view of extrinsic transformations. Note that overlapping transformations, namely os_sensor, os_imu and vectornav are omitted, while cam1, cam2 and cam3 are slightly pivoted downwards.

Table 4. RMSE of horizontal, vertical and rotational positioning errors.

| Method | Horizontal [m] | Vertical [m] | Rotational [°] |
|---|---|---|---|
| Leica GS18 (RTKLib RTK) | 2.416 | 5.003 | N/A |
| Leica GS18 (Net_Diff RTK) | 1.709 | 4.805 | N/A |
| Leica GS18 (Ginan PPP) | 2.385 | 5.720 | N/A |
| Leica GS18 (Ginan RTK) | 2.975 | 5.956 | N/A |
| UBLOX F9P (RTKLib RTK) | 16.840 | 23.717 | N/A |
| FAST-LIO2 | 58.162 | 40.730 | 6.210 |
| KISS-ICP | 78.300 | 48.566 | 6.606 |
| KISS-SLAM | 32.582 | 55.129 | 4.200 |
| PIN-SLAM | 32.075 | 49.432 | 4.156 |

However, the large errors near the middle of the data collection in Figure 7 suggest that the drifts are still profound when there is no nearby loop closure. It is therefore recommended for mapping tasks to distribute multiple loop closure locations throughout the trajectory for improved accuracy, as done in trip *20241114_3* (Figure 4).

## 6. Limitations

Melbourne Multi-Sensor Urban Positioning and Mapping Dataset is our first attempt at creating a positioning and mapping dataset that is modern, requires minimal data preprocessing or adaptation and can address multiple types of research developments. We have made several compromises due to various constraints, which should be made aware to the users of this dataset and improved in future work. First, the ground truth coordinates in this dataset are generated using the internal processing of the VectorNav VN300 INS. Although considered tactical-grade and highly accurate, it is not as widely accepted as a ground truth provider as more high-end systems such as the Novatel SPAN-CPT commonly used in other similar datasets. This could have impacted the accuracy of the ground truth information provided in our dataset. Second, apart from the cameras on the mobile mapping platform, the sensors are not hardware synchronised to accurate GPS timestamps as done in, e.g., UrbanNav (Hsu et al., 2023) and NavINST (Araujo et al., 2025). Since the GPS timestamps are recorded by the INS and all the sensors are synchronised to the system time using ROS2, this means that a time offset needs to be considered while integrating the multi-sensor data. However, using the Pulse-Per-Second (PPS) signal for more accurate synchronisation should be considered in the future. Third, due to the limited vehicle options, we employed a utility vehicle for the data collection, which has a large physical footprint. This mostly impacted the view of the front camera, which suffers from the occlusion of the car roof despite having been extended by over 0.5 m. Finally, we only collected night data and repeated trips on the *20241020* route. Providing more of such data can be a worthwhile addition to the dataset, as well as image and point cloud annotations of objects such as vehicles, pedestrians and road surface defects to extend the scope of the dataset to computer vision tasks.

## 7. Conclusions

This paper introduces the Melbourne Multi-Sensor Urban Positioning and Mapping Dataset, a new resource for research on multi-sensor integrated vehicle positioning and mapping in challenging urban environments. The dataset is built around a custom-made mobile mapping platform carrying a tactical-grade INS, dual-frequency and triple-frequency GNSS receivers, a high-resolution lidar and four industrial cameras providing 360° coverage. The sensor suite was deployed on inner-suburban streets in Melbourne, Australia, where dense buildings cause GNSS signal degradation, and closed loops and repeated trajectories were included to facilitate loop-closure-based SLAM and repeatability studies. All raw data are recor-


Figure 4. Ground truth trajectories (WGS84) of the data collection trips in Melbourne suburbs.

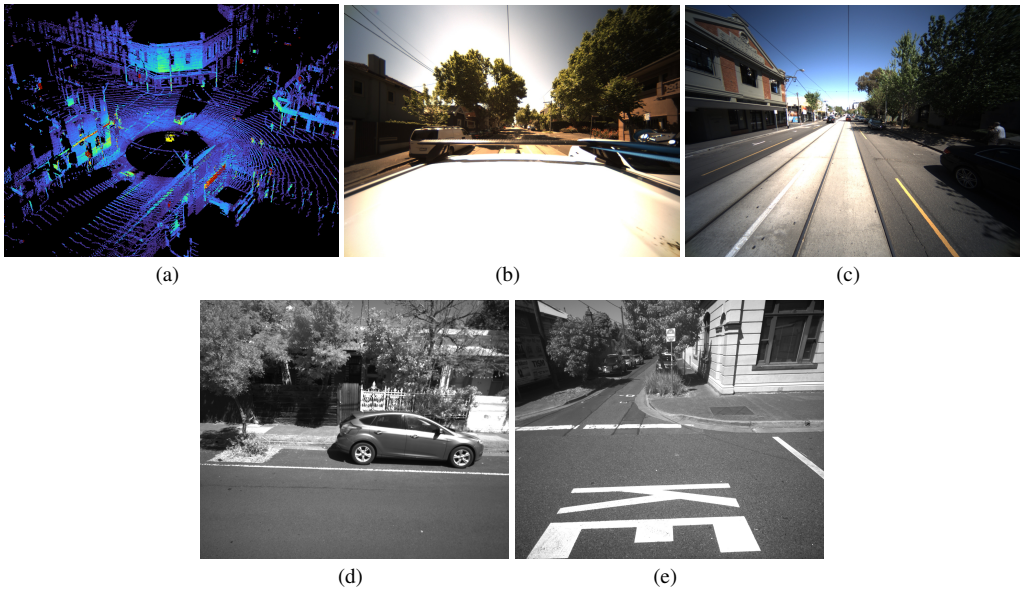


Figure 5. Samples of visual data. (a) Lidar (b) Front camera (c) Back camera (d) Left camera (e) Right camera

ded as standard ROS2 message streams in MCAP files and supplemented with widely used individual formats such as PCD, BMP, CSV and RINEX, as well as CORS observations and SSR precise products for GNSS processing.

The utility of the proposed dataset has been demonstrated by benchmarking three GNSS–based positioning packages and four state-of-the-art lidar(–inertial) odometry/SLAM systems. The results confirm that survey-grade GNSS can still provide metre-level accuracy in dynamic urban scenarios, while low-cost GNSS hardware remains significantly more susceptible to multipath and poor signal quality. Meanwhile, lidar–based methods produce smooth trajectories that are not correlated with instantaneous satellite visibility but exhibit drifts over time, particularly when loop closures are sparse. These complementary results highlight the continuing importance of tightly coupled sensor fusion and of dataset designs that include both challenging GNSS conditions and opportunities for global consistency through loop closures. More importantly, these experiments have shown the robustness and compatibility of the dataset with modern positioning and mapping workflows. With this contribution, we hope to support the development and validation of next-generation positioning and mapping algorithms by providing a data framework with complete multi-sensor inputs and minimal preprocessing overhead.

## References

Araujo, P. R. M. D., Mounier, E., Bader, Q., Dawson, E., Kaoud Abdelaziz, S. I., Zekry, A., Elhabiby, M., Noureldin, A., 2025. The NavINST Dataset for Multi-Sensor Autonomous Navigation. *IEEE Access*, 13, 84659–84674. https://ieeexplore.ieee.org/document/10980246.

Budiyono, A., 2012. Principles of GNSS, inertial, and multi-sensor integrated navigation systems. *Industrial Robot: An International Journal*, 39(3).

Caesar, H., Bankiti, V., Lang, A. H., Vora, S., Liong, V. E., Xu, Q., Krishnan, A., Pan, Y., Baldan, G., Beijbom, O., 2020.

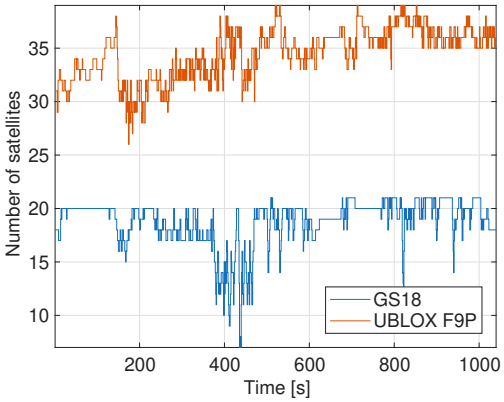


Figure 6. Number of satellites observed by Leica GS18 and UBLOX F9P throughout data collection.

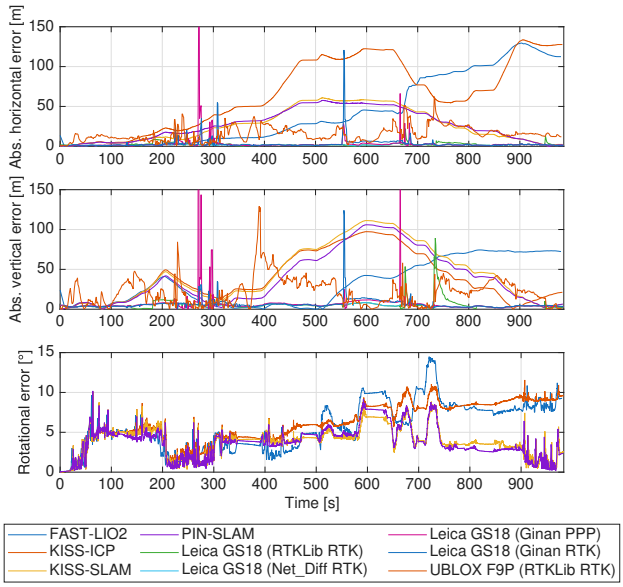


Figure 7. Absolute horizontal, vertical and rotational errors over time.

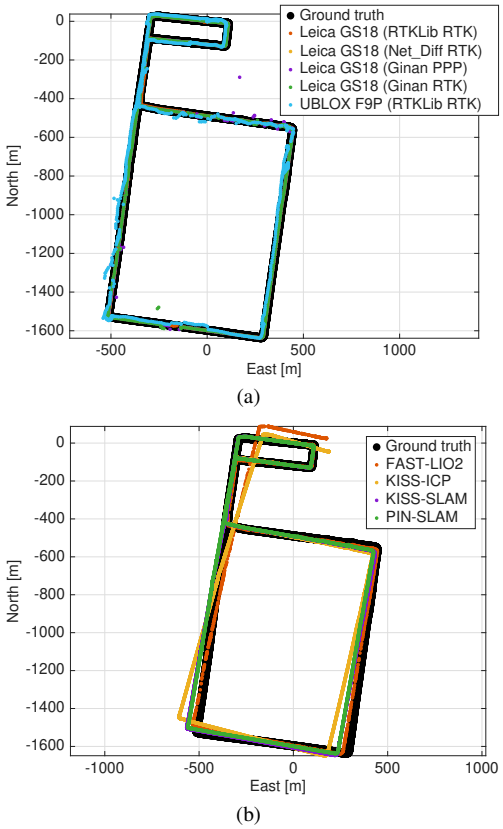


Figure 8. 2D positioning results. (a) GNSS–based (b) lidar–based

nuScenes: A multimodal dataset for autonomous driving. *2020 IEEE/CVF Conference on Computer Vision and Pattern Recognition (CVPR)*, 11618–11628. ISSN: 2575-7075.

Cao, S., Lu, X., Shen, S., 2022. GVINS: Tightly coupled GNSS–visual–inertial fusion for smooth and consistent state estimation. *IEEE Transactions on Robotics*, 38(4), 2004–2021.

Carlevaris-Bianco, N., Ushani, A. K., Eustice, R. M., 2016. University of Michigan North Campus long-term vision and lidar dataset. *The International Journal of Robotics Research*, 35(9), 1023–1035. https://doi.org/10.1177/0278364915614638.

Chen, P., Guan, W., Huang, F., Zhong, Y., Wen, W., Hsu, L.-T., Lu, P., 2023. ECMD: An Event-Centric Multisensory Driving Dataset for SLAM. *IEEE Transactions on Intelligent Vehicles*, 1–10. https://ieeexplore.ieee.org/abstract/document/10342726.

Geiger, A., Lenz, P., Stiller, C., Urtasun, R., 2013. Vision meets robotics: The KITTI dataset. *The International Journal of Robotics Research*, 32(11), 1231–1237. https://doi.org/10.1177/0278364913491297.

Guadagnino, T., Mersch, B., Gupta, S., Vizzo, I., Grisetti, G., Stachniss, C., 2025. KISS-SLAM: A Simple, Robust, and Accurate 3D LiDAR SLAM System With Enhanced Generalization Capabilities. *arXiv preprint*, arXiv:2503.12660. https://arxiv.org/pdf/2503.12660.

Hsu, C.-C., Huang, Y.-E., Chiang, K.-W., Tsai, M.-L., Chu, C.-H., 2025. Real-Time Precision Navigation Design for Autonomous Vehicle with EGI System. *The International Archives of the Photogrammetry, Remote Sensing and Spatial Information Sciences*, XLVIII-G-2025, 633–640. https://isprs-archives.copernicus.org/articles/XLVIII-G-2025/633/2025/.

Hsu, L.-T., Huang, F., Ng, H.-F., Zhang, G., Zhong, Y., Bai, X., Wen, W., 2023. Hong Kong UrbanNav: An Open-Source Multisensory Dataset for Benchmarking Urban Navigation Algorithms. *NAVIGATION: Journal of the Institute of Navigation*, 70(4). https://navi.ion.org/content/70/4/navi.602.

Ibrahim, M., Akhtar, N., Jalwana, M. A. A. K., Wise, M., Mian, A., 2021. High definition LiDAR mapping of Perth CBD. *2021 Digital Image Computing: Techniques and Applications (DICTA)*, 01–08.

Koide, K., Oishi, S., Yokozuka, M., Banno, A., 2023. General, Single-shot, Target-less, and Automatic LiDAR-Camera Extrinsic Calibration Toolbox. *2023 IEEE International Conference on Robotics and Automation (ICRA)*, 11301–11307.

Macenski, S., Foote, T., Gerkey, B., Lalancette, C., Woodall, W., 2022. Robot Operating System 2: Design, architecture, and uses in the wild. *Science Robotics*, 7(66), eabm6074. https://www.science.org/doi/abs/10.1126/scirobotics.abm6074.

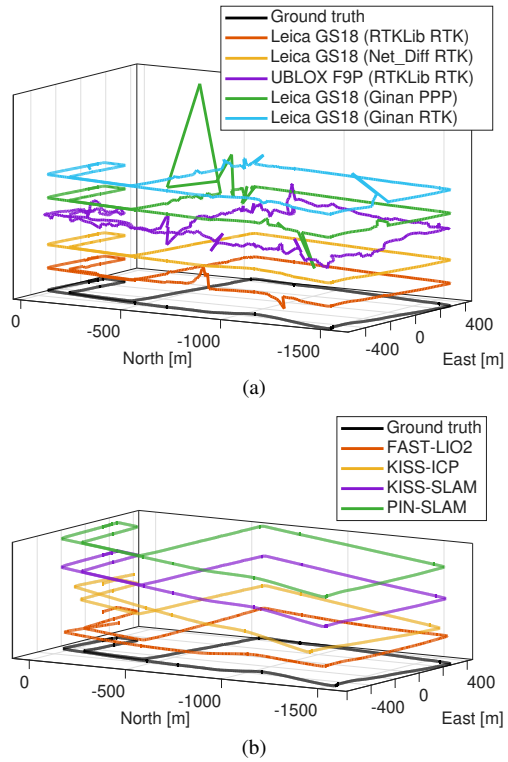


Figure 9. 3D positioning results. (a) GNSS–based (b) lidar–based

Maddern, W., Pascoe, G., Linegar, C., Newman, P., 2017. 1 year, 1000 km: The Oxford RobotCar dataset. *The International Journal of Robotics Research*, 36(1), 3–15. https://doi.org/10.1177/0278364916679498. Publisher: SAGE Publications Ltd STM.

McClusky, S., Hammond, A., Maj, R., Allgeyer, S., Harima, K., Yeo, M., Du, E., Riddell, A., 2024. Precise Point Positioning with Ginan: Geoscience Australia’s Open-Source GNSS Analysis Centre Software. *ION 2024 Pacific PNT Meeting*, 248–280.

Pan, Y., Zhong, X., Wiesmann, L., Posewsky, T., Behley, J., Stachniss, C., 2024. PIN-SLAM: LiDAR SLAM Using a Point-Based Implicit Neural Representation for Achieving Global Map Consistency.

Ramezani, M., Khoshelham, K., 2018. Vehicle positioning in GNSS-deprived urban areas by stereo visual-inertial odometry. *IEEE Transactions on Intelligent Vehicles*, 3(2), 208–217.

Schaper, A., Schön, S., 2024. Multi-agent multi-sensor collaboration for improved positioning in urban environment. *Proceedings of the 37th International Technical Meeting of the Satellite Division of The Institute of Navigation (ION GNSS+ 2024)*, 2780–2792.

Shan, T., Englot, B., 2018. Lego-loam: Lightweight and ground-optimized lidar odometry and mapping on variable terrain. *2018 IEEE/RSJ international conference on intelligent robots and systems (IROS)*, IEEE, 4758–4765.

Sun, P., Kretzschmar, H., Dotiwalla, X., Chouard, A., Patnaik, V., Tsui, P., Guo, J., Zhou, Y., Chai, Y., Caine, B., Vasudevan, V., Han, W., Ngiam, J., Zhao, H., Timofeev, A., Ettinger, S., Krivokon, M., Gao, A., Joshi, A., Zhang, Y., Shlens, J., Chen, Z., Anguelov, D., 2020. Scalability in perception for autonomous driving: Waymo open dataset. *2020 IEEE/CVF Conference on Computer Vision and Pattern Recognition (CVPR)*, 2443–2451. ISSN: 2575-7075.

Takasu, T., Yasuda, A., 2009. Development of the low-cost RTK-GPS receiver with an open source program package RTKLIB. *International symposium on GPS/GNSS*, 1, International Convention Center Jeju Korea Seogwipo-si, Republic of Korea, 1–6.

Vizzo, I., Guadagnino, T., Mersch, B., Wiesmann, L., Behley, J., Stachniss, C., 2023. KISS-ICP: In Defense of Point-to-Point ICP – Simple, Accurate, and Robust Registration If Done the Right Way. *IEEE Robotics and Automation Letters*, 8(2), 1029–1036.

Wang, Y., Tian, Y., Chen, J., Xu, K., Ding, X., 2024. A survey of visual SLAM in dynamic environment: The evolution from geometric to semantic approaches. *IEEE Transactions on Instrumentation and Measurement*, 73, 1–21.

Xu, W., Cai, Y., He, D., Lin, J., Zhang, F., 2022. FAST-LIO2: Fast Direct LiDAR-Inertial Odometry. *IEEE Transactions on Robotics*, 38(4), 2053–2073. https://ieeexplore.ieee.org/document/9697912.

Yin, J., Li, A., Li, T., Yu, W., Zou, D., 2022. M2DGR: A Multi-Sensor and Multi-Scenario SLAM Dataset for Ground Robots. *IEEE Robotics and Automation Letters*, 7(2), 2266-2273.

Zhang, J., Khodabandeh, A., Khoshelham, K., 2023a. On the role of lidar measurements in speeding up precise point positioning convergence. *GPS Solutions*, 27(3), 149. https://doi.org/10.1007/s10291-023-01497-3.

Zhang, J., Khoshelham, K., Khodabandeh, A., 2023b. Fast converging lidar-aided precise point positioning: A case study with low-cost GNSS. *ISPRS Annals of the Photogrammetry, Remote Sensing and Spatial Information Sciences*, X-1-W1-2023, 687–694. https://isprs-annals.copernicus.org/articles/X-1-W1-2023/687/2023/.

Zhang, Y., Chen, J., Gong, X., Chen, Q., 2020. The update of BDS-2 TGD and its impact on positioning. *Advances in Space Research*, 65(11), 2645-2661. https://www.sciencedirect.com/science/article/pii/S0273117720301666.

Zhang, Y., Kubo, N., Chen, J., Wang, J., Wang, H., 2019. Initial Positioning Assessment of BDS New Satellites and New Signals. *Remote Sensing*, 11(11). https://www.mdpi.com/2072-4292/11/11/1320.

Zhao, J., Zhao, W., Deng, B., Wang, Z., Zhang, F., Zheng, W., Cao, W., Nan, J., Lian, Y., Burke, A. F., 2024. Autonomous driving system: A comprehensive survey. *Expert Systems with Applications*, 242, 122836.

Zhu, F., Ren, Y., Zhang, F., 2022. Robust Real-time LiDAR-inertial Initialization. *2022 IEEE/RSJ International Conference on Intelligent Robots and Systems (IROS)*, 3948–3955. ISSN: 2153-0866.